International Journal of Mechanical Sciences 188 (2020) 105944

Contents lists available at ScienceDirect

International Journal of Mechanical Sciences

journal homepage: www.elsevier.com/locate/ijmecsci

Influence of inlet and outlet placement on the hydrodynamics of culture tanks for Atlantic salmon

JMR Gorle[a,*], BF Terjesen[a,†], ST Summerfelt[b,‡]

[a] Nofima AS, Sunndalsøra 6600, Norway
[b] The Conservation Fund Freshwater Institute, 1098 Turner Road, Shepherdstown, WV 25443, USA

ARTICLE INFO

Keywords:
Recirculation aquaculture system (RAS)
Hydrodynamics
Inlet and outlet location
Eulerian-lagrangian approach
Self-cleaning

ABSTRACT

The salmon farming industry has recently shifted to larger culture tanks with greater water flows to optimize the land-based production, but tanks approaching 1000 m^3 in volume create challenging hydrodynamics. This paper presents a computational study of four combinations of inlet and outlet designs of a commercial land-based aquaculture tank. Windows-based OpenFOAM solvers are used to solve the conservation equations for tank hydrodynamics with an implicit unsteady second-order Eulerian (finite volume) technique on unstructured hybrid meshes. The model is validated by the velocity measurements at discrete locations in the tank using acoustic doppler velocimetry. To understand the dispersion of biosolids in the tank, 500 particles with a uniform size of 200 μm are tracked in the Lagrangian frame. While the tank's Reynolds number varies between 2E6 - 3.5E6 depending on the flow exchange rate, the local Reynolds number at the inlet pipe is about 2E5 which discovers the drag-crisis phenomenon. The effect of inlet and outlet placement on the velocity, vorticity and turbulence is addressed. The existing tank design could be improved using the bottom-drain and corner-inlet options, which strengthens rotational flow with better uniformity. Such design change is also proved to provide better particle removal and thus ensure the improved self-cleaning ability of the tank.

1. Introduction

With Recirculating Aquaculture Systems (RAS), the aim is to create controlled rearing conditions so that disease outbreaks are prevented, fish performance is improved, waste streams are managed so that nutrients can be reclaimed, and water consumption is minimized [12,53,55]. The Norwegian salmon industry has been experiencing a steady increase in the implementation of RAS technology for the past three decades, primarily for production of approximately 100 g smolt that is subsequently stocked into ocean pens for culture to generally 4–5 kg at harvest. More recently, however, the Norwegian Ministry of Fisheries has allowed the production of even larger smolt or post-smolt up to 1000 g in tanks, before stocking in the sea, which has created an opportunity for Norwegian industry to increase the investment in such facilities [29]. Today, by contributing about 30% to the Norwegian salmon smolt production, RAS facilities experience increased reliability and production efficiency, versus older flow-through systems in which the water is only used once. Increasingly, there are also initiatives in several countries to use RAS to culture salmon all the way to harvest size. However, RAS is still a new technology and much research effort is needed to ensure acceptable reliability and efficiency. For instance, the current lack of a rational-based design approaches and characterization of pertinent flow physics results in an uncertain hydraulic system of the culture tanks, where in fact the fish resides. The general information on water velocity and pressure fields is not sufficient to explore the opportunities of improving the large constructions of RAS culture tanks, which today can be 1000 m^3 and larger [51]. The benefits of increased biosecurity through RAS technology can only be exploited when the proper hydraulic setting is implemented; otherwise fish performance (growth, feed utilization, survival), welfare, and health will suffer. Correct hydrodynamics in the culture tank is crucial to achieving the desired rotational velocity in the tank for improved fish exercise and health [23,26,60], optimum mixing characteristics for better water quality [2,57,59] and uniform flow pattern to avoid quiescent zones and rapidly flush settleable solids from the culture tank [15].

Abbreviations: ADV, acoustic doppler velocimetry; CFD, computational fluid dynamics; DNS, direct numerical simulation; GAMG, geometric agglomerated algebraic multigrid; HRT, hydraulic retention time; RAS, recirculating aquaculture system; RANS, Reynolds averaged Navier-Stokes; RNG, *Re*-normalisation group; SIMPLE, semi-implicit method for pressure linked equations; TKE, turbulent kinetic energy; TSS, total suspended solids (ppm).

* Corresponding author.
E-mail address: gorle.jmr@gmail.com (J. Gorle).
† Current address: Cermaq Group AS, Dronning Eufemias gt 16, N-0102, Oslo, Norway
‡ Current address: Superior Fresh LLC, W15506 Superior Fresh Drive, Hixton, WI 54,635 USA

https://doi.org/10.1016/j.ijmecsci.2020.105944
Received 31 March 2020; Received in revised form 12 July 2020; Accepted 13 July 2020
Available online 15 July 2020

Nomenclature

A	area (m^2)
C_1, $C_{1\varepsilon}$, C_2, $C_{3\varepsilon}$, C_μ	model constants of Realizable $k-\varepsilon$ model
C_d	drag coefficient
C_f	skin-friction coefficient
d	particle diameter (m)
D	mean diameter of the tank (m)
$\mathbf{D}$	stretching tensor
f_p	force exerted on particle (N)
g	acceleration due to gravity (m/s^2)
h	water column height in the tank (m)
I	identity matrix
T_i	turbulence intensity
k	turbulent kinetic energy (m^2/s^2)
m	particle mass (kg)
p	pressure (pa)
G_k, G_b	production terms of TKE
R	tank radius (m)
Re	reynolds number
R_h	hydraulic radius of the tank (m)
S_{ij}	deformation tensor
S_k, S_ε	user-defined source terms of k and ε
St	stokes number
t	time (s)
t_e	eddy life time (s)
t_{int}	particle-eddy interaction time (s)
t_p	particle relaxation time (s)
t_{tr}	transit time of the particle through the eddy (s)
v	velocity (m/s)
$\bar{v}$ and v'	mean and fluctuating velocity components
ϑ	particle volume (m^3)
v_0	inlet nozzle velocity (m/s)
v_p	particle velocity (m/s)
x_p	particle displacement (m)
$y+$	non-dimensional wall distance

Greek symbols

γ	flow uniformity index
Γ	vortex strength (J)
δ	kronecker Delta
ε	dissipation rate of turbulent kinetic energy (m^2/s^3)
μ	dynamic viscosity (Pa.s)
μ_t	turbulent viscosity (Pa.s)
ν	kinematic viscosity (m^2/s)
ρ	water density (kg/m^3)
ρ_p	particle mass density (kg/m^3)
σ_k, σ_ε	model constants of Realizable $k-\varepsilon$ model
τ	viscous stress tensor
τ_w	wall-shear stress (Pa)
ω	angular velocity (rad/s)
Ω_{ij}	rotation tensor

In practice, each plug of flow injected into a large culture tank has its own residence time, which depends on inflow and outflow momentum, flow turbulence, and internal design of the tank including the placement of inlet and outlet structures. The result is a non-uniform flow domain including low-momentum zones in the tank. Considerable effect of inlet and outlet characteristics on the global flowfield has been found in many bioresource systems such as bioreactors [35], biofilters [8], and flow columns [1]. However, the existing literature in aquaculture research fails to address the effect of such design parameters on the tank hydrodynamics, let alone improve them.

The rotational velocity in a culture tank, which implicitly depends on inlet flowrate and hence the impulse force plays an important role in creating a healthy rearing environment [14,26,42,44]. Flow pattern and turbulence in the tank are primarily influenced by the inlet and outlet characteristics [25,27,28,34,39]. Other than these authors, different inlet and outlet configurations in RAS tanks have been used in past studies but most of it has been ad-hoc research. In the development of an integrated recirculating aquaculture and olericulture plant, McMurtry et al. [36] used a free-fall inflow model, and the water was drawn by means of a pump from the bottom of the tank using a pipe. In a recirculation system for oyster larval culture, Qiu et al. [45] used a suspended inlet and central elevated outlet. However, a tangential inlet flow and central bottom drain have been the most common flow boundaries in several studies [46,49,50]. The physiological studies of Davidson et al. [16] and Good et al. [22] deployed circular RAS tanks with tangential inlet and Cornell type dual-drain system. Indeed, the combination of a central bottom outlet and an elevated wall drain is often used in circular RAS tanks to achieve a controlled flow pattern. However, the location of the inlet and outlet structures affect the hydrodynamics of large culture tanks.

An empirical investigation on the water velocities in large circular and octagonal RAS tanks with tangential inlet nozzles was performed by Gorle et al. [26]. The authors found that circular tanks, which had a central bottom outlet, experienced approximately 50% lesser variation in water velocity at the centre, compared to octagonal tanks that had a central top outlet. Also, both tanks appeared to have different velocity profiles across the tank. The octagonal tanks used in the fish performance studies of Espmark et al. [19] had the inlet pipe near the corner wall. Such design aspects of flow boundaries considerably influence the overall hydrodynamics of the tank, which cannot be ignored when trying to improve the environmental conditions for the fish.

The usual placement of the inlet pipes in land-based RAS facilities is near the tank's periphery to ensure that a stronger rotational flow occurs, but this will, in turn, cause a flow resistance due to the structural obstruction in the highest velocity region. The net drag force on the inlet pipe is the sum of friction drag and form drag. Form drag, characterised by vortex shedding and flow separation, is a dominant component in such bluff bodies like a circular cylinder at high Reynold numbers. In RAS culture tanks, the mean hydraulic retention time of 30 - 55 min. is the preferred water exchange rate for sufficient water quality for the fish. The rotational flow past the inlet pipes at these operating conditions results in a Reynolds number of approximately 2E5. At this critical Reynolds number, the drag force on a smooth cylinder abruptly drops. The present explanatory analysis of the inlet pipe location excludes the physics of the 'drag-crisis phenomenon', as named by Schlichting [47]. Out of numerous flow control techniques, 'blowing' is an active method where the flow separation zone on the leeward side of the cylinder is reenergized by streaming a jet through an orifice. The bluff body hydrodynamics associated with the flow past an inlet pipe is characterized by a low-pressure wake region on the rear side of the cylinder. The pressure drag is a dominant component, which can be reduced up to 65% by modifying the geometry of base flow [3,7]. 'Jet blowing' has been widely studied in different applications to energize the recirculation zone [31,56], and thus reduce the drag force of the body. Representation of these dynamic features around the inlet pipe and the effect of its location was not made by previous studies in the case of culture tanks.

A circular flow pattern with dominant tangential velocity in circular or octagonal culture tanks translates the linear water inflow into a rotating vortex flow [39,40]. One of the most critical features of a central outlet in a confined flow domain is the evolution of locally organized coherent structures at a wide range of length scales [27,28], which dominate the turbulence transport mechanisms like skin friction, mixing, etc. The experimental observations of such phenomena involve huge costs and efforts and often deliver uncertain outcomes [37]. On the other hand, a simulation-driven development provides a less-costly vir-

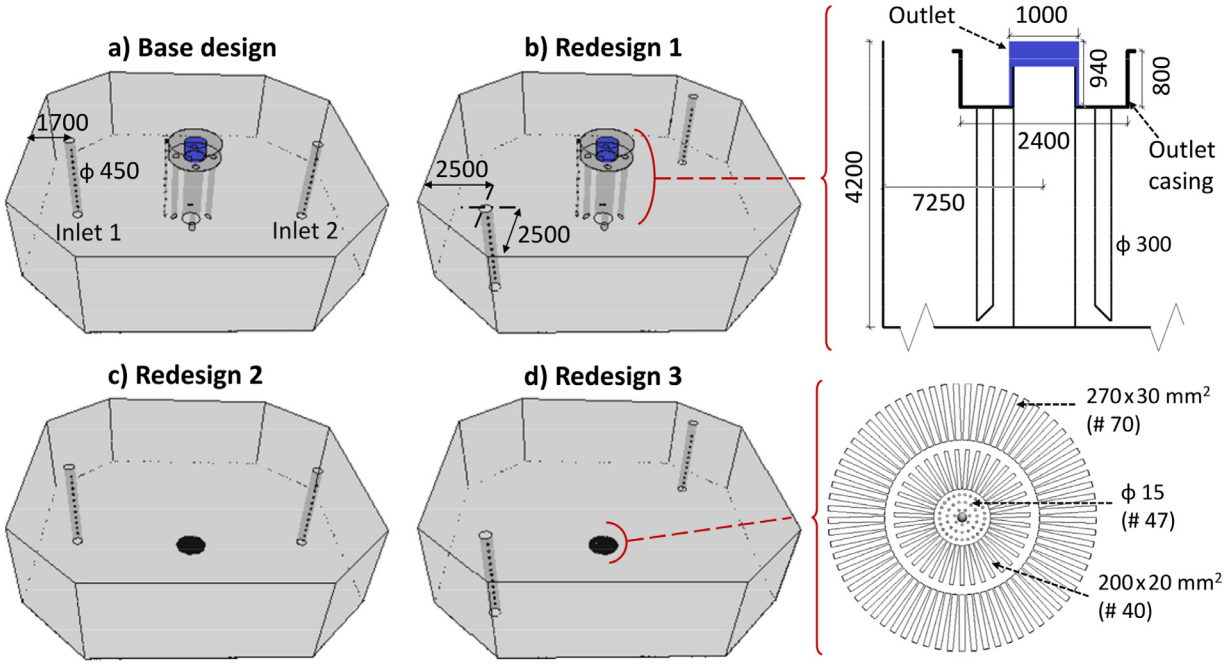

Fig. 1. Tank designs for computational flow analysis. (a) Base design with the inlet pipes at sidewalls, and (b) Redesign 1 with the inlet pipes near the corner walls of the tank. In both designs, the flow in the tank reaches the elevated central outlet (in blue colour) through four vertical pipes; the basic dimensions of this outlet system are given in the top-right drawing. (c) and (d) show the redesigns 2 and 3, which have identical inlet systems as in Base design and Redesign 1, respectively, but the elevated outlet is replaced by the conventional slotted outlet at the bottom of the tank. The design specifications of the central bottom outlet are shown in zoomed view on the right-bottom corner.

tual environment to understand physics and improve the design, thanks to high-performance computing. In this study, an octagonal shaped commercial RAS tank of 788 m^3 size was investigated using turbulence modelling. In addition to the Base design, three design variants in terms of inlet and outlet locations are considered in this study to examine the qualitative and quantitative parameters of Atlantic post-smolt tank hydrodynamics. The novelty of the study is that the flow physics behind the rotating turbulent flow associated with the culture tanks is explored. The combined vortical-streamlined-vectorial representation explains the flowfield structure near different outlets. Better inlet placement in the tank is studied based on the force estimates. This research also quantifies the effect of inlet/outlet locations on the field variables including flow velocity, uniformity, circulation, and the motion of the biosolids in the tank. In the long-term, such studies can improve RAS energy, bioresource use, and fish performance, health, and welfare in aquaculture.

2. Numerical methodology

2.1. Designs under study

Optimization of large flow domains, such as culture tanks of close to 1000 m^3 in volume, is not straight forward because the optimal solutions, as functions of design and operating conditions, cannot be found by simple numerical programming. An exhaustive search for a perfectly optimized tank design over a full set of continuous variables involves rigorous computational effort and thus offers an impractical method. A comparative study between a few selected solutions is instead a more effective and time-saving method. Our earlier research on an octagonal RAS tank of 788 m^3 size investigated the effect of the inlet nozzle angle on the tank's performance [28]. While the same design was taken as reference i.e *base design*, this study considered three additional combinations of inlet-outlet locations as presented in Fig. 1.

- ***Base design*** (Fig. 1a), which is currently in operation at a Norwegian smolt producer, has two inlet pipes near the sidewalls. Each inlet pipe has 11 nozzles that discharge the water into the tank parallel to the sidewalls so that a clockwise flow pattern develops when viewed from the top. The tank has an elevated outlet at the centre, which collects the water near the floor of the tank through four vertical pipes around it. The effective inlet and outlet surface areas are 0.0226 m^2 and 2.95 m^2, respectively.
- ***Redesign 1*** (Fig. 1b) has the same outlet as the Base design but the inlet pipes were moved close to the near the corner walls. The distance from the corner wall to the pipe's centre is 1.49 m and that to the tank's centre is 8.2 m. Thus, the redesign follows the inlet pipe location at 1/5th of radial distance from the corner wall in NCRA's RAS tank in Norway [19,55]. The nozzle configuration on the pipes and inflow direction are the same as the Base design.
- ***Redesign 2*** (Fig. 1c) has the inlet pipes near the sidewalls, as in Base design, but here the complex central elevated outlet was replaced by a simple bottom drain, as used by Summerfelt et al. [52] and Davidson and Summerfelt [14]. The outlet consists of 47 exit nozzles of 15 mm diameter each, surrounded by two radially patterned rectangular slots. The effective outlet surface area was reduced from 2.95 m^2 in the elevated drain to one-fourth in the bottom drain.
- ***Redesign 3*** (Fig. 1d) has the inlet pipes near the corner walls and a central bottom drain.

The aforementioned tank designs were tested for practical flow conditions, as obtained from the commercial salmon site, using the computational fluid dynamics. This research considered the tanks with no biomass and hence the analysis of biosolids was not in the scope of the study. Through flow blockage, the fish response to velocity and vorticity increases the overall turbulence. However, the relative comparison between the tank designs can be equally valid for the tanks with biomass.

2.2. CFD modelling

A cost-effective computational framework was developed for the high-fidelity CFD simulations. The tank geometries were developed using CATIA V5 R21 (Dassault Systèmes, Vélizy-Villacoublay, France). The

fluid domain was extracted in the STEP format to effectively transfer the CAD metadata structures for robust interoperability between different software platforms. 3D-Tool V12 (3D-Tool GmbH & Co. KG, Weinheim, Germany) was used to translate the STEP file into a Parasolid format to make it compatible with the meshing tool. An automated meshing tool, Castnet (DHCAE Tools GmbH, Krefeld, Germany), was employed for finite volume-based domain discretization. After a thorough checked for different quality parameters, the mesh was imported into the CFD tool, BlueCFD (BlueCAPE, Casais da Serra, Portugal), which offers Windows version of OpenFOAM solvers along with a graphical interface, called RunGui. The results of coupled Eulerian-Lagrangian simulations for the hydrodynamics and particle dispersion in the culture tank were then post-processed in Paraview 5 (Kitware, New York, USA) and Matlab R17 (MathWorks, Natick, Massachusetts, USA). The details of model equations and problem setup are presented in this section.

2.2.1. Continuous phase

The modelling of the flow domain in the RAS tank was performed in a three-dimensional unsteady incompressible framework with the RANS-based turbulence model. The mass and momentum conservation equations are

$$\nabla . v = 0 \tag{1}$$

$$\frac{Dv}{Dt} = -\frac{1}{\rho}\nabla p + \nu\,\nabla^2 v \tag{2}$$

where v is the velocity field, ρ, p and ν represent the density, pressure and kinetic viscosity of the fluid, respectively. Using the Reynolds decomposition of instantaneous velocity v into average ($\bar{v}$) and fluctuating (v') components, the Eq. (2) becomes

$$\frac{D\overline{v_j}}{Dt} = -\frac{1}{\rho}\frac{\partial \bar{p}}{\partial x_j} + \nu\,\nabla^2\overline{v_j} - \frac{\partial \overline{v_i v_j}}{\partial x_i} \tag{3}$$

where $\tau(=\overline{v_i v_j})$ is the Reynolds stress term. The closure approximation in RANS modelling to eliminate fluctuating velocity v' yields

$$\tau = \frac{2}{3}k\mathrm{I} - \nu_t D \tag{4}$$

where $k(=\frac{1}{2}\overline{|v'|^2})$ is the turbulent kinetic energy, I is the identity matrix, ν_t is the eddy viscosity and D is the averaged stretching tensor, defined by $\frac{1}{2}(\mathrm{grad}\,\bar{v}+{}^t\mathrm{grad}\,\bar{v})$. Using the hypotheses of gradient diffusion and eddy viscosity, the momentum equation becomes

$$\dot{\bar{v}} = -\frac{1}{\rho}\mathrm{grad}\left(\bar{p} + \frac{2}{3}\rho k\right) + \left(\nu + \nu_t\right)\Delta\bar{v} \tag{5}$$

Although numerous models exist to solve the transport equations for k and relevant scalar variables, each has some advantages and limitations depending on the application. For industrial cases, the two-equation models that solve the equations for k and its dissipation rate ε are more popular due to their robustness, computational feasibility, and reasonable accuracy. In this study, the realizable $k-\varepsilon$ model is used which enforces the realizability on the formulation of μ_τ by relating the model constant to the strain tensor. The model respects the binding constraints of Reynolds stresses and realizes the physics of turbulent flows. This is more significant in accurately modelling the flow features such as rotations and vortices; the critical aspects of culture tank hydrodynamics. The conservation equations for k and its dissipation rate ε therefore become

$$\rho\frac{\partial}{\partial x_j}\left(k v_j\right) = \frac{\partial}{\partial x_j}\left[\left(\mu + \frac{\mu_t}{\sigma_k}\right)\frac{\partial k}{\partial x_j}\right] + G_k + G_b - \rho\varepsilon + S_k \tag{6}$$

$$\rho\frac{\partial}{\partial x_j}\left(\varepsilon v_j\right) = \frac{\partial}{\partial x_j}\left[\left(\mu + \frac{\mu_t}{\sigma_\varepsilon}\right)\frac{\partial \varepsilon}{\partial x_j}\right] + \rho C_1 S_\varepsilon - \frac{\rho C_2 \varepsilon^2}{k+\sqrt{\nu\varepsilon}} + C_{1\varepsilon}\frac{\varepsilon}{k}C_{3\varepsilon}G_b + S_\varepsilon \tag{7}$$

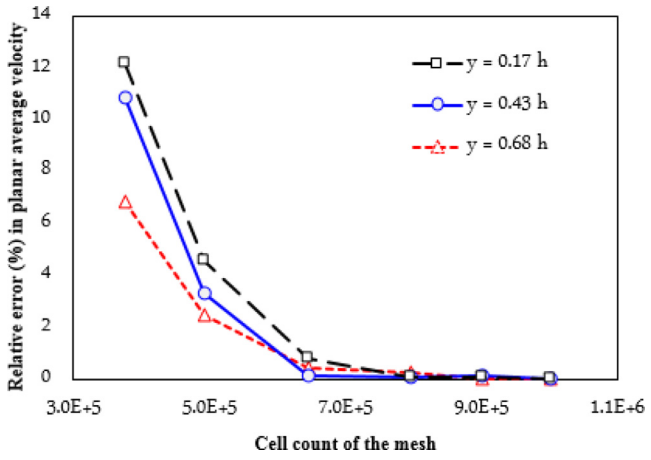

Fig. 2. Mesh dependency of average velocity across the planes at 17%, 43% and 68% of the water column height.

where $C_1 = \max[0.43, \frac{\eta}{\eta+5}]$, $\eta = \frac{k\sqrt{2S_{ij}S_{ij}}}{\varepsilon}$ and $S_{ij} = \frac{1}{2}(\frac{\partial v_j}{\partial x_i} + \frac{\partial v_i}{\partial x_j})$. G_k and G_b represent the generation of turbulent kinetic energy due to average velocity gradients and buoyancy, respectively. S_k and S_ε are the user-defined source terms, and the model constants are $C_{1\varepsilon}$=1.44, C_2=1.9, σ_k=1.0 and σ_ε=1.2. Although the turbulent viscosity $\mu_t(=\rho C_\mu \frac{k^2}{\varepsilon})$ is computed same as in other $k-\varepsilon$ models, the difference arises from the calculation of C_μ. While the Standard and RNG models assume C_μ to be constant, the realizable model defines it as

$$C_\mu = \frac{\varepsilon}{4.04\varepsilon + \sqrt{6}k\cos\theta\sqrt{S_{ij}S_{ij} + \tilde{\Omega}_{ij}\tilde{\Omega}_{ij}}} \tag{8}$$

where $\tilde{\Omega}_{ij} = \bar{\Omega}_{ij} - 3\varepsilon_{ijk}\omega_k$. The inclusion of mean rate-of-rotation tensor $\bar{\Omega}_{ij}$ along with strain rates, angular velocity ω and the turbulence parameters k and ε,in the definition of C_μ and hence in the computation of μ_t makes the realizable $k-\varepsilon$ model more superior than the standard and RNG models in predicting the spreading of round jets from the inlet nozzles of a culture tank. In addition, the transport equation for ε considers the transport of the mean-square vorticity fluctuation, which made the model the means of turbulence modelling in the current study.

2.2.2. Dispersed phase

The motion of the biosolids in the rearing domain is explored by means of Lagrangian particle tracking method. Uneaten feed pellets and faecal matter are the usual contributors of suspended solids in the culture tanks. The particle dispersion in Lagrangian frame is computed from the Eulerian flow field, and the particle motion is governed by

$$\frac{dx_p}{dt} = v_p \tag{9}$$

$$m\frac{dv_p}{dt} = \sum f_p \tag{10}$$

where f_p is the force experienced by the particle of diameter d, mass m when it has a velocity v_p at position x_p and time t.

The presence of the any particulate matter in the culture tanks is critical to water quality and hence the fish growth. However, the volume ratios of the biosolids in the tanks are very small. For instance, Davidson et al. [13] shows that the total suspended solids (TSS) in culture tanks can range from 2.8± 0.2 ppm to 18.2± 5.9 ppm depending on the water exchange rate and the use of flow-flow ozonation. Also, [26] reported the TSS accumulation in different Norwegian commercial smolt tanks, ranging from 2.1± 0.5 to 12.1± 4.0 ppm in various tanks at the time of sampling. In such dilute suspensions, the particle-particle interaction and the effect of particle motion on the

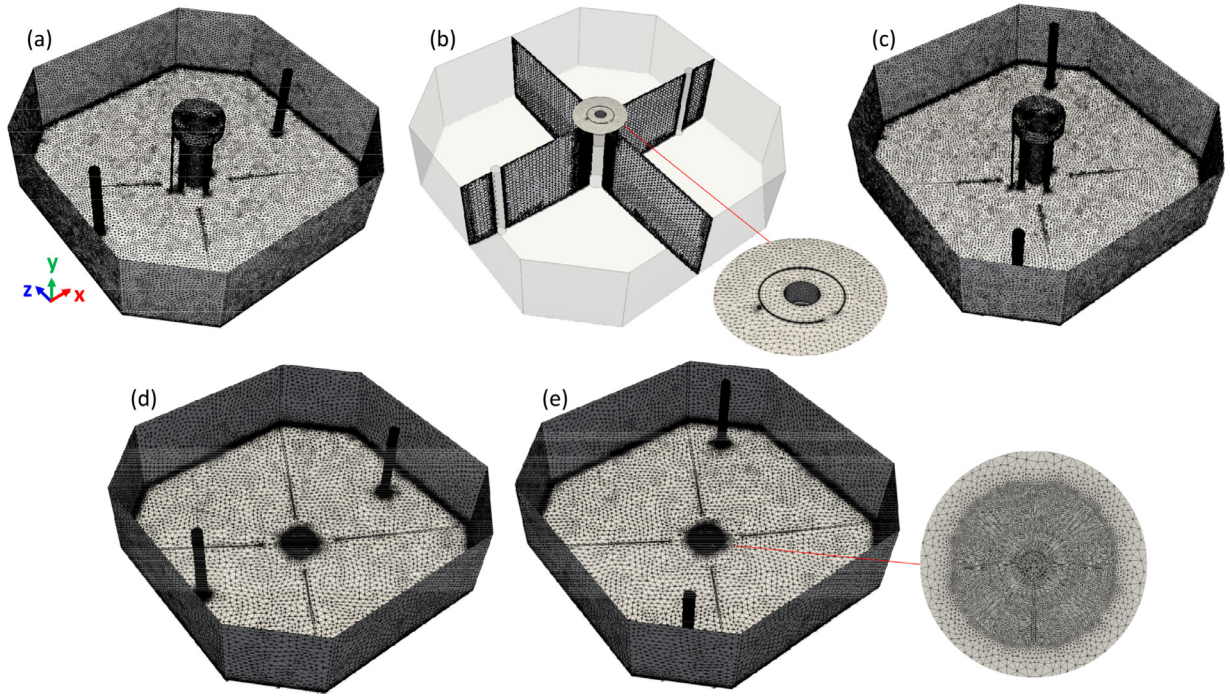

Fig. 3. Mesh visualization on the selected geometries. (a) Unstructured triangular cells on the surface, and (b) hexahedral mesh in the core of the Base design with an enlarged view of the near-casing surface mesh. Similar discretization strategy was adopted for other designs as well. (c), (d) and (e) show the surface meshes for the redesigns 1, 2 and 3 with the zoom-in view of the clustered cells near the bottom outlet of Redesign 3.

flow and turbulence are negligible [18]. The influence of fluid motion on the particles can be characterised by the Stokes number according to

$$St = \frac{\rho_p d^2 v}{18 \mu L} \tag{11}$$

where ρ_p and d are the density and diameter of the particles, v is the flow, μ is the dynamic viscosity of the fluid and L is the characteristic length, which is the mean diameter of the tank in the present case. While the size of particles in culture tanks ranges from nano to millimetres, this study considered 200 μm uniformly sized rigid spherical particles. These specifications correspond to $St << 1$ which represents the interaction between the flow and particles is one-way, i.e., from the former to the latter [10,21].

Although the consideration of lift terms on the particles of different sizes in turbulent flows has long been a topic of debate [33,58], numerous studies on Lagrangian particle tracking ignored the lift terms when the particle diameter is sufficiently small (for instance, [4,56]). Ignoring the pressure and added mass forces along with the Basset history term for the sake of simplicity for a relative comparison between the tank designs, the dominant forces on the particle are drag f_d, buoyancy and gravitational force f_g i.e., $\sum \mathrm{f}_p = \mathrm{f}_d + \frac{(\rho_p - \rho)\pi d_p^3 g}{6}$. The particles were assumed to have the drag components due to sphere drag and gravity. Therefore, the particle drag becomes

$$\mathrm{f}_d = \frac{3m\mu C_d Re_p}{4\rho_p d^2}(v - \mathrm{v}_p) + \frac{\pi \rho_p d^3}{6} g \tag{12}$$

where $Re_p (= \frac{d|v - \mathrm{v}_p|}{v})$ is the particle Reynolds number, ρ_p is the particle density, v is the flow velocity and g (= 9.81 m/s^2) is the gravitational acceleration, respectively. Assuming the constant mechanical properties, the particle drag coefficient C_d is defined by

$$C_d = \begin{cases} \frac{24}{Re_p} \text{ for } Re_p \le 0.5 \\ \frac{24}{Re_p}\left(1 + 0.15 Re_p^{0.687}\right) \text{ for } 0.5 \le Re_p \le 1000 \\ 0.44 \text{ for } Re_p > 1000 \end{cases} \tag{13}$$

The particle trajectory is computed within the turbulent field using the random-walk algorithm [5] where the particle position is updated at every time-step using the eddy-interaction model. Denoting the particle variables which are derived from the interpolation of Eulerian field at adjacent cells by the subscript p^+, the effect of eddies on the particle's velocity is considered by adding the local fluctuating velocity component v'_{p^+}. Therefore, the effective particle velocity becomes $\tilde{\mathrm{v}}_{p^+} = \mathrm{v}_{p^+} + \mathrm{v}'_{p^+}$. The fluctuating velocity component is calculated from

$$\mathrm{v}'_{p^+} = \varphi \sqrt{\frac{2}{3}k} \tag{14}$$

where ϕ is a random number generated from Gaussian probability distribution with null mean and unit variance, and $\sqrt{\frac{2}{3}k}$ is the local RMS flow velocity fluctuations. A DNS correction factor is used in the stochastic model to counter the presumed isotropic turbulence within the boundary layer region. The transit time of the particle to travel through the eddy (t_{tr}) and the eddy life time (t_e) are determined from

$$t_{tr} = -t_p \ln\left(1 - \frac{l_e}{\tau_p \left|\tilde{\mathrm{v}}_{p^+} - \mathrm{v}_p\right|}\right) \tag{15}$$

$$t_e = \frac{C_\mu^{0.63} \frac{k^{1.5}}{\varepsilon}}{\left|\mathrm{v}'_{p^+}\right|} \tag{16}$$

Here, $t_p (= \frac{4}{3}\frac{\rho_p d}{\rho C_d |v - \mathrm{v}_p|})$ is the particle relaxation time to respond to the changes in the local flow. The particle-eddy interaction time is calculated from $t_{int} = \min(t_{tr}, t_e)$. Then, the particle's position and velocity at the n^{th} Lagrangian time step are computed from

$$\mathrm{x}_p^{t + \sum_{t=1}^{n} \Delta t_i} = \mathrm{x}_p^{t + \sum_{t=1}^{n-1} \Delta t_i} + \mathrm{v}_p^{t + \sum_{t=1}^{n-1} \Delta t_i} \Delta t_n \tag{17}$$

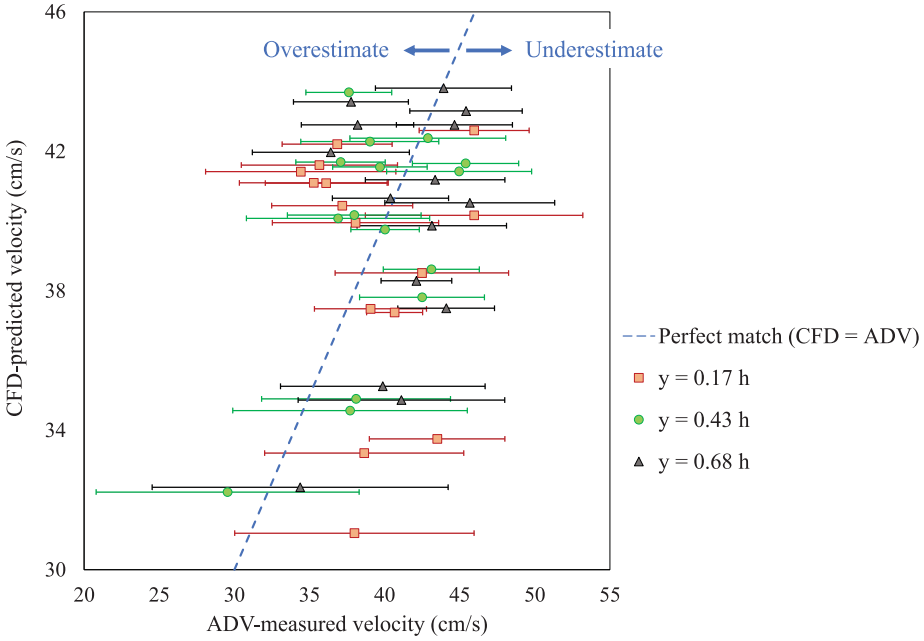

Fig. 4. Comparison between the computationally predicted and ADV-based measurements of velocity at different locations across three vertical locations i.e. 17%, 43% and 68% of water column height.

$$v_p^{t+\sum_{t=1}^{n}\Delta t_i} = \frac{v_p^{t+\sum_{t=1}^{n-1}\Delta t_i} + v_{p+}^{t}\frac{\Delta t_n}{\tau_p} + g\Delta t_n}{1+\frac{\Delta t_n}{\tau_p}} \tag{18}$$

2.3. Domain discretization

The undesired entities such as slivers, small faces and open edges were removed, and the geometry was simplified using the built-in utilities of the meshing tool. Several meshes were created by changing the global cell size to evaluate mesh dependency. Several mesh quality parameters were thoroughly checked for each mesh using the built-in mesh-check utility. The convergence criterion of 1E-5 was set for the relative error in the computation of velocity magnitude. A series of mesh convergence tests on the Base design of the tank was conducted by refining the global cell size. Fig. 2 shows the mesh dependency results of the Base design for the average planar velocity at three heights of the water column where the empirical measurements were taken. The final mesh on the Base design had 797,819 unstructured finite volumes and any further size refinement produced an error smaller than 0.2% relative to the last refined mesh. This hybrid mesh containing the tetrahedral cells on solid boundaries and hexahedral cells in the core, as shown in Fig. 3(a) and 3(b) respectively, offers the advantage of negotiating the complex geometrical features with high-quality cell distribution at the reasonable computational effort. Four inflation layers with a height ratio of 1.15 were used to capture the velocity gradients in the near-wall region. The resulting the non-dimensional wall distance $y+$ was above 30, and standard wall functions were used to compute the near-wall effects [43]. Although highly skewed cells don't hamper to solution stability, these, however, reduce the order of face integration. The final mesh had the cell skewness below 0.5. Over 95% of the cells had the dihedral angle between 70° and 120°, and 98% of the domain had the cell aspect ratio below 5 which ensured adequate mesh quality. For more details on the mesh topology and grid dependency results, please refer to our previous publication [28]. Similar topological settings were used to produce the meshes for the redesigns 1, 2 and 3 which created the final grids with the cell-counts of 796,226, 779,812 and 779,991, respectively. These surface mesh visuals are presented in Fig. 3(c-e).

2.4. Boundary conditions and problem setup

The nozzles on the inlet pipes were assigned 'mass flow' boundary conditions, and the tank's outlet acted as 'outflow' boundary. All solid surfaces of the tank were defined as 'no-slip' smooth static walls which take zero-gradient condition for k, ε and p. Free-surface deformation in the tank is negligible due to the continuous replenishment of water into the tank with the same flowrates through the inlet and outlet boundaries [28]. Assuming a turbulence intensity T_i of 5%, the initial k and ε were calculated from $k = 1.5(T_i\bar{v})^2$ and $\varepsilon = c_\mu k^2/5\nu$. Time-dependant segregated viscous solver with second-order Gaussian linear discretisation for both convective and diffusive terms was used in the simulations. The pressure-velocity equations were coupled using SIMPLE (Semi-Implicit Method for Pressure Linked Equations) algorithm. While the pressure equation was solved with GAMG (geometric agglomerated algebraic multigrid) formulation, all other field equations were solved using Gauss– Seidel based smoothSolver. A constant time-step of 0.01 s was used with 30 inner-iterations. Simulations were run in parallel mode on a 28-core Intel Xeon E5-2683v3 2.00 GHz computer.

3. Results and discussion

3.1. CFD model validation

The CFD model of the Base design for validation was developed for an inflow of 292 kg/s. The Reynolds number is calculated from

$$Re = \frac{4R_h\rho V}{\mu} \tag{19}$$

where the hydraulic radius $R_h(=\frac{Rh}{R+2h})$ is a function of tank's equivalent radius R (=8.15 m) and h is the height of water column (=3.9 m). Therefore, a mean retention time of 45 min, in this case, corresponds to Re of 2.3E6. The velocity measurements were taken at predefined locations in the salmon culture tank when operated without fish. A Nortek high-resolution acoustic Doppler profiler, *Vector*, was used for the measurements at 45 discrete locations in the tank across three heights, i.e., 17% and 43% and 68% of the water column. The validation of the CFD model using the velocity measurements in Fig. 4 shows that the simulation results largely fall within the standard deviation bars of the ADV findings. The latest developments of transducers have reduced the

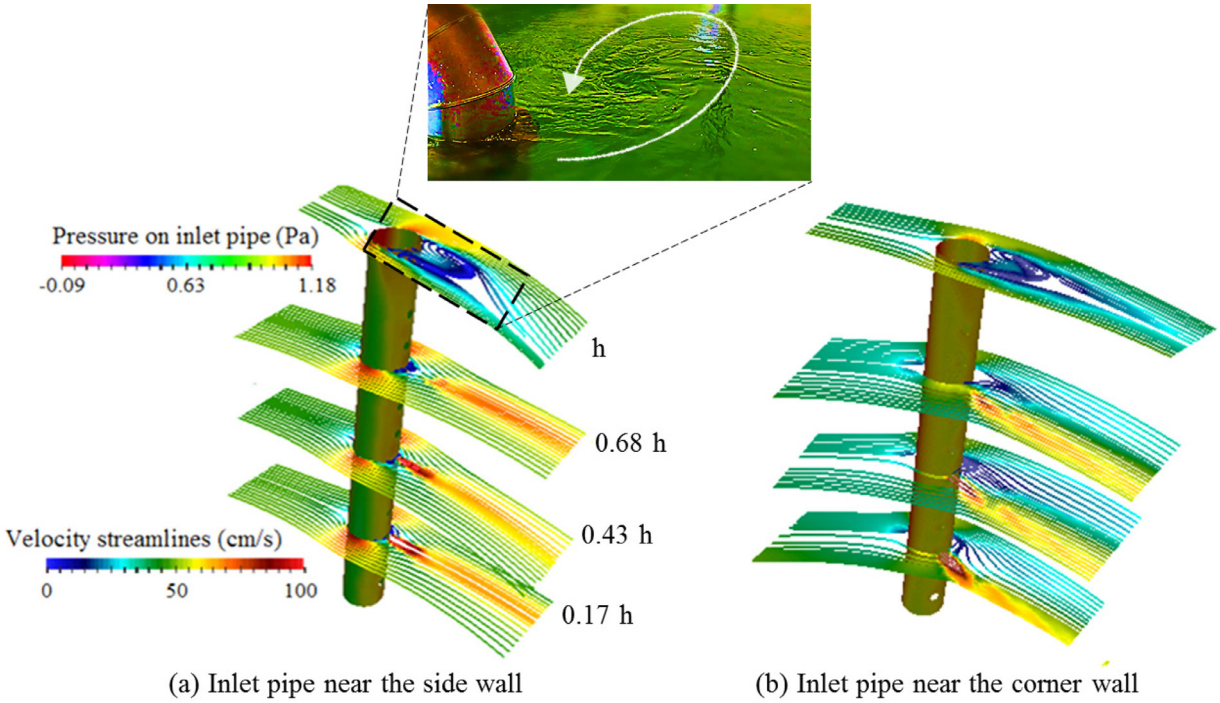

Fig. 5. Flow pattern around the inlet pipe, when placed near the sidewall (left) and corner wall (right). Streamline distribution is plotted at four heights for a water column height, h, of 3.9 m. Flow direction is from left to right.

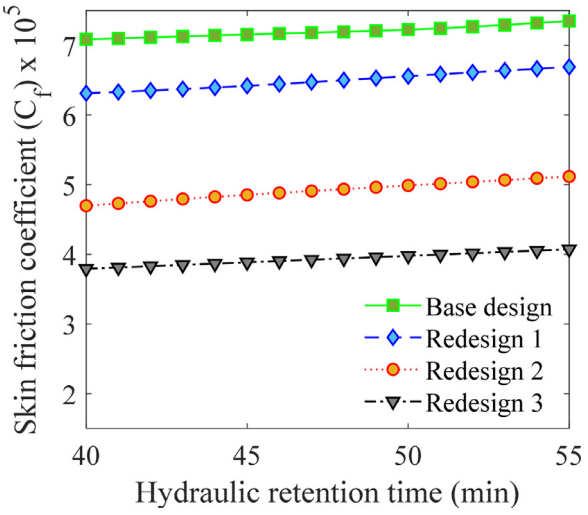

Fig. 6. Variation of skin-friction coefficient, C_f, with the mean hydraulic retention time of different tank designs.

blanking distance of modern ADV instruments to as low as 5 cm. However, the effect of flow disturbances, both due to the domain turbulence and the instrument inducement, on the performance of these transducers challenge the measurement accuracy [17]. Also, the Doppler noise is likely to influence the peak velocities recorded by the ADV module. Despite that low-quality data was removed by the signal filtering process, the signal aliasing was expected to combine with the Doppler noise and velocity fluctuations, which possibly influence the ADV measurements in the turbulent flows in a RAS tank. A correlation coefficient above 90% and signal-to-noise ratio of more than 15 dB was achieved with a sampling frequency of 25 Hz. The resulting coefficient of variation is approximately 7% and the average difference between the ADV and CFD results is 9%. This, along with our previous research [25–27], highlights that ADV and CFD methods complement each other more than validate one another. For more details on the measurement setup, and the validation of velocity trends and flow angles across the tank, please refer to Gorle et al. [28].

3.2. Flow field around the inlet pipe

Previous studies have determined that the rotational velocity at the perimeter of circular tanks is strongly dependant upon the impulse force of water flow injected tangentially into the circular-type tank. Thus, the rotational velocity depends upon the hydraulic exchange rate and inlet nozzle velocity and the direction produced at the flow inlet structures. Fundamentally, the inlet pipe in the culture tank conditions for the problem of flow around a circular cylinder, which is one of the standard cases of fluid mechanics. In octagonal tanks, the flow near the corner walls turns into itself to negotiate its path with the tank walls. Therefore, the inlet pipes in the tank redesigns 1 and 3 experience a manoeuvring flow, represented by curvilinear streamlines in Fig. 5(b). This has a significant effect on the locations of stagnation points, pressure distribution and wake formation, compared to the case of straight flow over the inlet pipes, i.e., the pipes near the sidewalls as in the Base design and Redesign 2. As a result, the pressure distribution on the pipe (partially shown in Fig. 5) is significantly different in both cases of inlet pipe location.

The distance of the tank's centre from the corner wall is 13% more than that from the sidewall, which causes the streamlines to spread more along the diagonals of the tank than along the *x*- or *y*-axis in a circular patterned flow. This means that the inlet pipe near the corner wall is exposed to a lower flow velocity (~15% lesser velocity) than those at the sidewalls. Using the empirical relationship between the drag force and Reynolds number, formulated by Cheng [9], the drag coefficient C_d of the inlet pipe with no jet from nozzles was found to be 1.206, which is consistent with the classical drag curve of a smooth cylinder [57]. With the jet blown at much higher velocities than base flow, Fre-

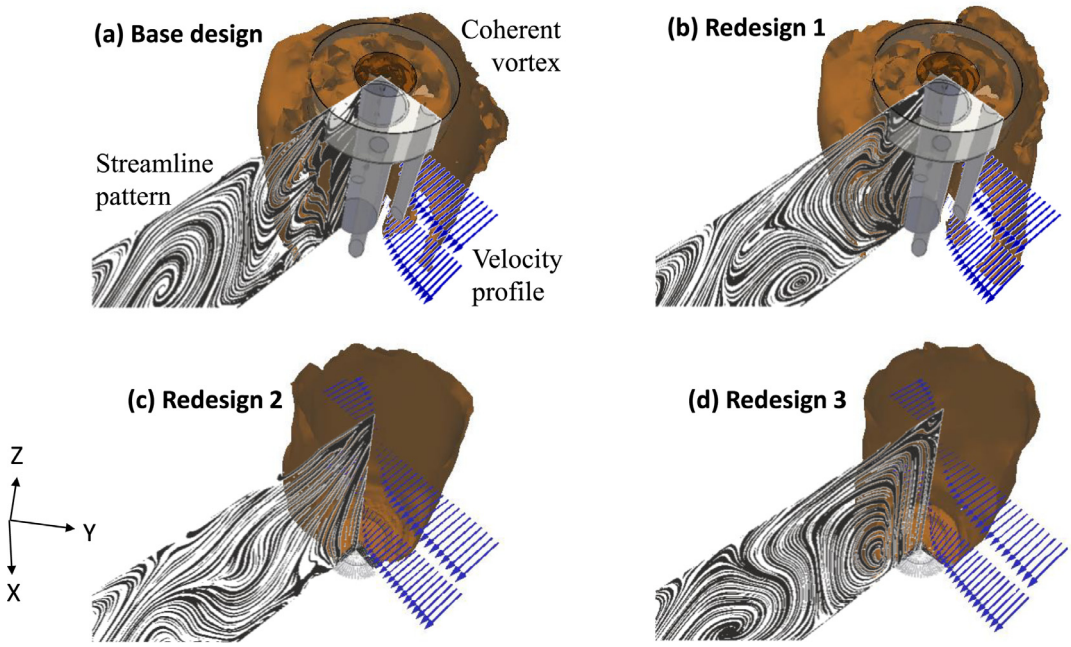

Fig. 7. Quarter-wedge sectional view of the vortex column formed in the four selected tank designs. Velocity profile and streamline patterns are shown across mutually perpendicular planes. The flow rate corresponds to a mean HRT of 45 min.

und and Mungal [20] achieved zero drag on the body of interest. In the present study, the inlet velocity for mean hydraulic retention time (HRT) in the tank of 40 min is 2.69 m/s, which is approximately 4 times larger than the mean rotational velocity when the inlet pipe is placed near the sidewall. As depicted in Fig. 5(a), the low-pressure wake region was replaced by a pressure recovery region, represented by the accelerated flow on the rear side of the pipe. Thus, the nozzle injection has greatly cancelled the drag force of the pipe by more than 99%. The nozzle flow from the inlet pipe near the corner wall is however not aligned with the base streamlines, resulting in an offset between the wake zone and peak velocity stream, as shown in Fig. 5(b). Hendrick and Degrez [30] highlighted the significant effect of jet location on the flow-induced forces. Consistent with this, a relatively weak suppression of the low-pressure region downstream of the pipe is observed. However, the low-velocity flow near the corner wall keeps the drag force of the pipe lesser than when placed near the sidewalls by 29% which makes it a better placement in terms of average velocity and hence energy use. Another advantage of corner wall positioning of the inlet pipe is that the low-velocity region gains additional momentum due to the structural obstruction as well as inlet flow, and hence increases the flow uniformity in the tank.

The effect of outlet location is associated with keeping or removing the complex central outlet system, which is present in the Base design and Redesign 2. With such a draining system, the flow has to travel more distance from inlet to outlet. In addition, the rotational flow around the central vertical pipes creates additional drag, compared to redesigns 1 and 3. The comparison between the designs for the skin-friction coefficient, which is defined as $C_f = \frac{\tau_w}{0.5\rho v^2}$ with τ_w being wall-shear stress, is shown in Fig. 6. With an elevated outlet, the inlet pipe near the corner wall (Redesign 1) experiences 10% lesser C_f than that near the sidewall (Base design), whereas this difference between the redesigns 2 and 3 becomes 20%. The reason for lesser C_f with Redesign 1 compared to the Base design is that the flow in the former has low energy loss to the walls from the base flow, which is also true for Redesign 3 compared to Redesign 2. Over 30% less C_f is observed with the replacement of complex central-top outlet by conventional bottom outlet. The Reynolds effect on the overall drag force is demonstrated by a slight but steady increase in C_f with HRT.

3.3. Flowfield near the outlet

Ideal axisymmetric vortices, governed by Burger's equation, are based on the assumption that the effects of axisymmetric straining and viscosity diffusion are balanced. This is not true in real flows, and therefore the cylindrical vortices are not perfectly axisymmetric. Detailed characterization of vorticity is imperative as it affects the global velocity field of the tank [27]. Fig. 7 shows the cut-away view of the vortex column prevailing at the centre in the selected tank designs. The resultant circular flow pattern is the combination of streamlines across the plane ?? = constant, a large-scale cylindrical vortex around the outlet, and the rotational flow, represented by vectors. Here, the isovortex surface was quantified by *Q*-criterion, which is defined by the positive second invariant of velocity curl ($\nabla x v$), Mathematically, $Q = |\Omega_{ij}|^2 - |S_{ij}|^2$, where Ω and S are the rotational and deformation components of velocity gradient respectively [24]. The size of the vortex column with conventional bottom outlet, as in redesigns 2 and 3, is approximately 22% lesser than the central top outlet due to the space occupied by the pipes in the tank's centre (Base design and Redesign 1).

3.4. Large-scale and small-scale turbulent structures

The evolution of turbulent structures at different length scales influences the global flowfield through vortex-vortex interaction, for example. The fine-scale coherent structures likely affect the dynamics of large-scale turbulence [11,48], which in turn affect the dispersion of particles in the wall-bounded flows [6]. Therefore, it is necessary to characterize the turbulent structures in the different designs of the culture tank. In this study, the small-scale turbulence was identified by coherent vortical structures, using *Q*-criterion while the turbulent kinetic energy defined by $k = 0.5\overline{v_i' v_i'}$ with v_i' being the fluctuating velocity component, was used to define the large-scale turbulent structures. As seen from Fig. 8, the intensity of the time-averaged vorticity increases with the hydraulic exchange rate. The vortex ring in mid-radius location, by receiving the turbulent energy from the base flow, seems to be moving faster and contributes to the motion of the vortex core. The size of the vortex ring is approximately 12% lesser in the designs with inlet pipe near the corner walls, compared to that near the sidewalls.

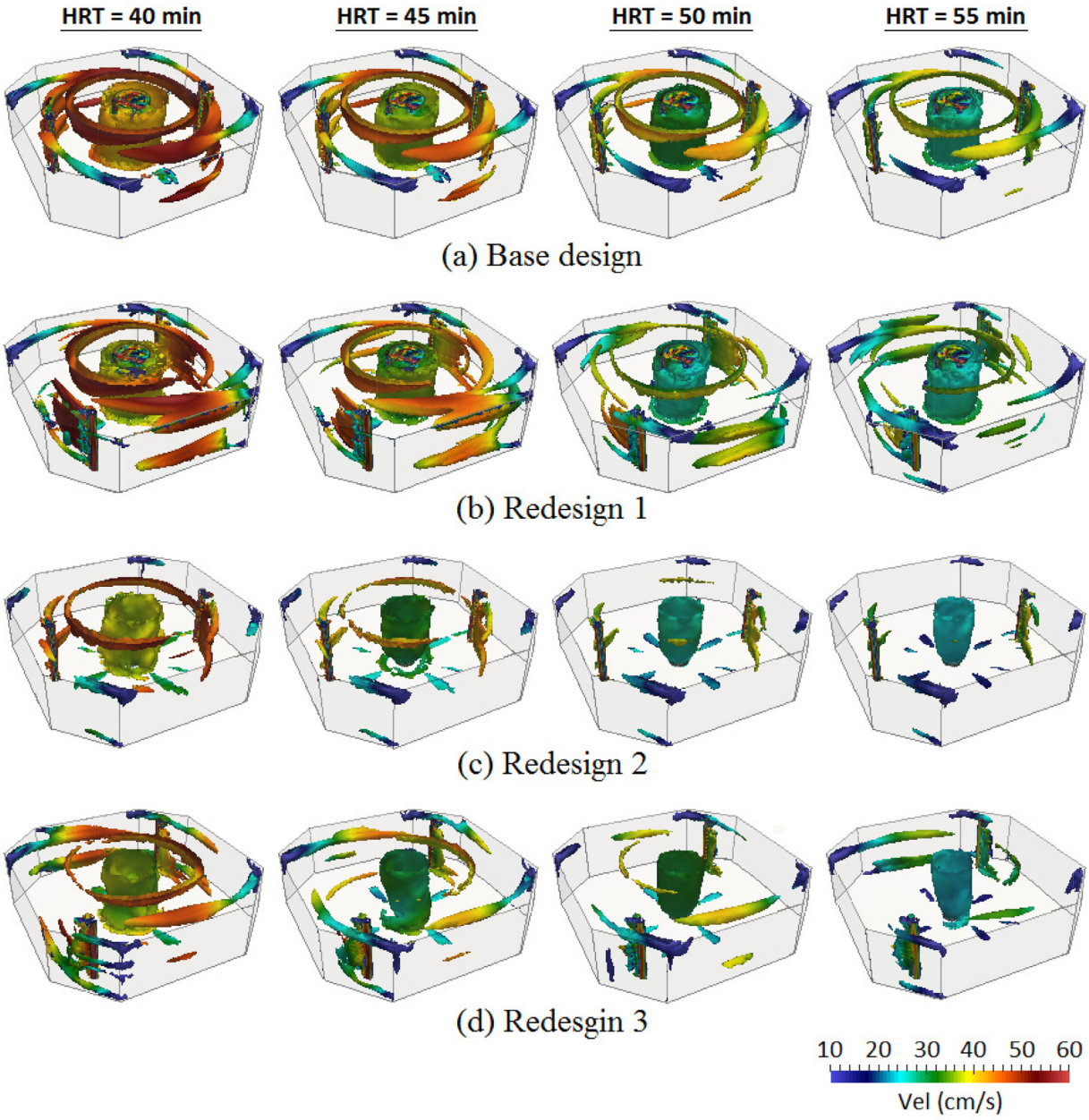

Fig. 8. Coherent vorticity distribution in the base design and redesigns for different operating conditions. Iso-surfaces of $Q = 0.01$ are coloured on velocity scale.

Fig. 9 shows the time-averaged distribution of turbulent kinetic energy (TKE) in the tank designs. On a general note, the TKE is not uniformly distributed throughout the domain. Mixing of inflow with the rotating flow in the tank creates the most intense turbulence, but further from this mixing region, the turbulence decays as the water spreads in the tank. Turbulence levels near the outlet are reasonably high due to the locally strained flow. Denser turbulent kinetic energy contours in the Base design, and redesigns 1 and 2, particularly at higher flow exchange rates, reveal the higher flow viscidity in the core of the tank. In particular, the higher TKE distribution in Base design explains that the flow pattern is more disorder and random, which is relatively negligible in redesigns 2 and 3. It can be concluded that the inlet pipes near the sidewalls and central top outlet configurations are more detrimental in terms of the flow uniformity and energy loss. The viscous effects in the conservation equations become dominant when the length scale of an eddy is adequately small. The turbulent kinetic energy is then quickly dissipated and therefore the nonuniformity of the flow vanishes. Thus, the dissipation rate of turbulent kinetic energy ε is a crucial parameter, which is governed by the dynamics of small-scale eddies. Fig. 10 compares the designs in terms of the time-averaged planar distribution of ε near the floor and water surface. Concentrated profiles of ε at the water surface in Base design and Redesign 1 explains higher turbulent diffusivity and hence better micromixing of the flow. On the other hand, the height-wise variation of ε in Redesign 2 is relatively negligible. The lowest amounts of TKE in Redesign 3 lead to low turbulent mixing and therefore low diffusion rate.

3.5. Performance metrics

The selected designs were further contrasted for three performance metrics; normalized rotational velocity (v/v_0), flow uniformity index (γ) and vorticity strength (Γ/Dv_0), where v_0 is the inlet nozzle velocity. These hydrodynamic indicators were evaluated at four inflow conditions of 328, 292, 263 and 239 kg/s, representing the mean hydraulic

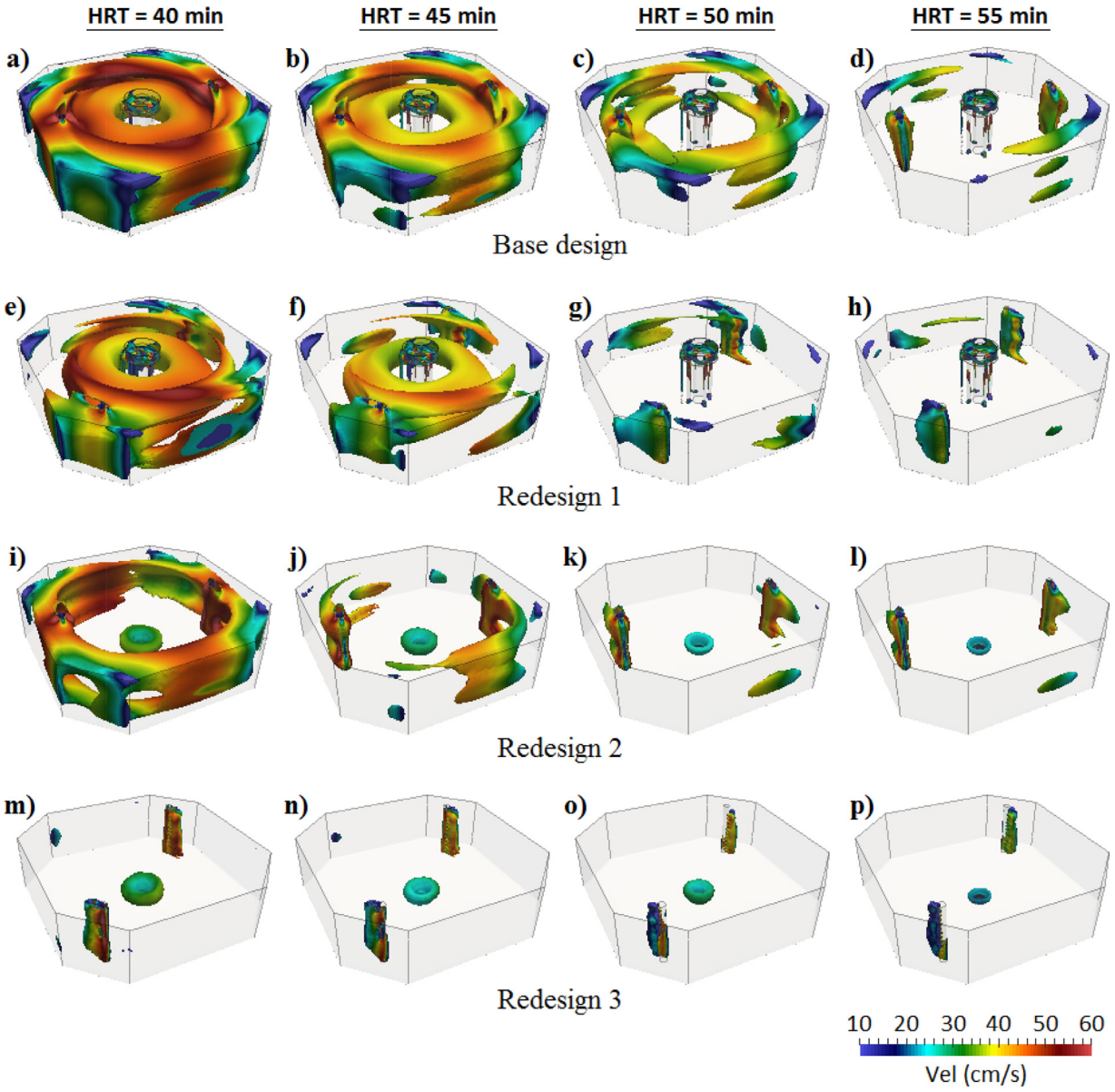

Fig. 9. Contours of turbulent kinetic energy, k, in base design and redesigns of the tank for different operating conditions.

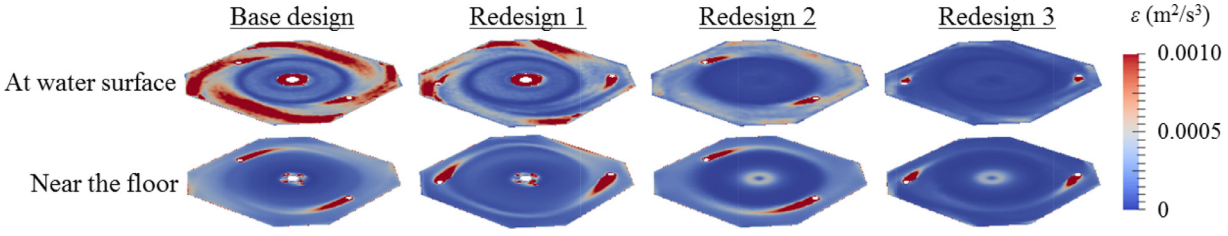

Fig. 10. Planar distribution of turbulent dissipation rate, ε, in the four tank designs for HRT = 40 min.

retention time of 40, 45, 50, and 55 min respectively, and Reynolds numbers ranging within 2E6 - 3.5E6. Recalling that the Base design and Redesign 1 have the central-top outlet, while redesigns 2 and 3 have the central-bottom outlet. As can be seen from Fig. 11, this classification was reflected in the velocity distribution in the tanks, and the placement of inlet pipes seems relatively inconsequential in this regard. The flow passages at the bottom and top of the outlet structure (i.e. 60% and 40%, respectively) in the Base case and Redesign 1 causes local accelerated regions, which leads to the peaks in the velocity profiles in Fig. 11(a) and 11(b). The confined flow geometry causes to spread the lower peak, i.e., at the bottom of the vertical outlet structure and negotiate with the adjacent velocity distributions, which resulted in a smooth velocity profile. The anomalous behaviour of the free-surface, however, limits this scenario for the flow through the casing channels, resulting in a near comparatively sharper velocity peaks. Replacing the complex central-top outlet system simply by holes on the floor at the tank's centre have

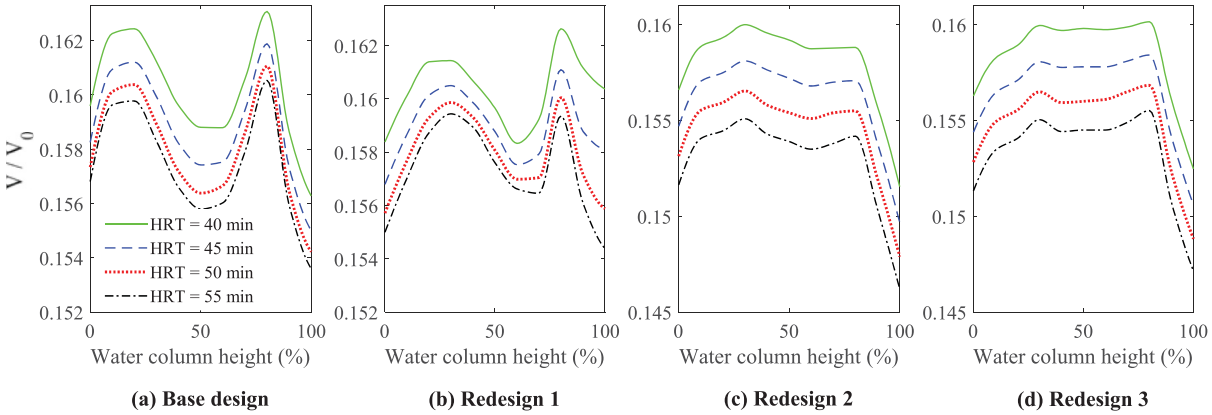

Fig. 11. Normalized velocity distribution across the tank with different inlet and outlet configurations.

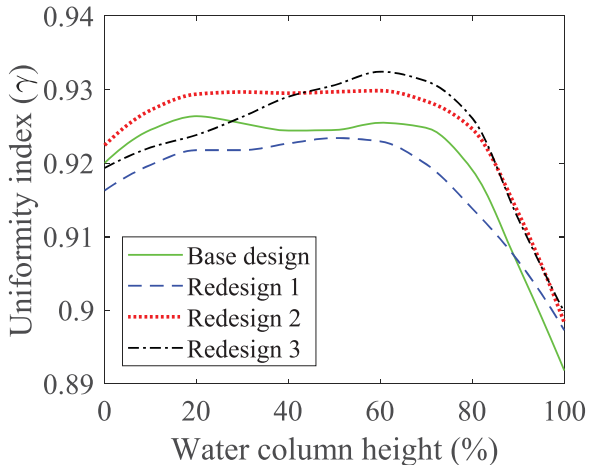

Fig. 12. Comparison between the selected designs for flow uniformity index γ for HRT = 45 min.

drastically changed the velocity trends, as depicted in Fig. 11(c) and 11(d). Except near the floor and water surface where stronger flow gradients exist, the velocity is more uniform across the tank height with the central bottom outlet. The increase in the velocity magnitude with decreasing HRT is linear with the bottom-outlet, which is not true with top-outlet. The trend of velocity change with the water exchange rate is hard to quantify due to the nonlinear nature of the velocity distribution in the case of the central-top outlet.

One of the objectives in the culture tank development is to achieve the maximum possible flow uniformity across the tank, which would result in more consistent water velocities for the fish. Because of non-uniformity associated with the vortices in the form of velocity gradients, the overall flow uniformity is affected by the increasing vortex intensity and turbulence, which is common in most fluidic systems (for example, [38,41]). The index γ was used in this study to quantify the flow uniformity in the tank. Mathematically, it is defined by

$$\gamma = 1 - \frac{1}{2nA}\sum_{i=1}^{n}\frac{\sqrt{(v_i - \bar{v})^2}}{\bar{v}}A_i \tag{20}$$

where n is the number of computational cells in the section of area A, v_i is the velocity in the cell, whose area is A_i and v is the area-weighted mean planar velocity. The index γ is computed across the horizontal plane at every 10% height and interpolated to construct the flow uniformity profile for the entire height of the water column. The comparison between the Base design and the redesigns in Fig. 12 reveals that the designs have different γ profiles across the tank's height. Irrespective of the design, the overall flow uniformity is always above 90%. A mere shift of inlet pipes from the sidewall location (Base design) to corner wall location (Redesign 1) causes the flow uniformity to drop by 2%. The optimum flow uniformity was achieved by Redesign 2, i.e., with the inlet near the sidewall and bottom drain while the lowest uniformity was found with Redesign 1, i.e., with inlet near the corner wall and elevated drain.

The flow features in the tank designs were further studied in terms of vortex strength, which is defined by $\frac{\Gamma=(\int_A \omega dA)}{Dv_0}$ where ω is the vorticity magnitude and D is the characteristic length. The convective and viscous terms in the momentum transport equation depend on the Reynolds number. Therefore, the vortex strength that dominates the mean flow varied with the inflow rate of the tank. As observed from Fig. 13, a gradual decrease in the vortex strength with increasing hydraulic retention time is observed with Base design and Redesign 1, whereas this drop is fairly constant in redesigns 2 and 3. This implies that the central bottom drain gives a more predictive performance than the central elevated drain, as vorticity distribution is concerned. Looking at the height-wise variation in the vortex strength, the central elevated drain yet again displays a highly non-linear distribution. The two peaks of the profiles in Fig. 13(a) and 13(b) represent increased vortex strength because of flow through four vertical pipes at 5 cm from tank's floor and 40% of the total flow through the openings of outlet casing near the water surface. In contrast, the vortex strength is more linearly distributed across the tank height in redesigns 2 and 3 (Figs. 13c and 13d). The location of the outlet surface grossly determines the vortex strength of the water surface; the closer the outlet to water surface, the higher the vortex strength would be.

The biosolids generated in the culture tank from the fish and biofilms need to be flushed rapidly as their hydrolysis leads to decomposition which decreases the dissolved oxygen levels and releases organic molecules, fine suspended solids and ammonia. Another danger that can occur in RAS using sea water is that toxic H2S can also accumulate in the tank, and it is likely that such a scenario is more probable if solids are not rapidly washed out [32]. To get rid of particle accumulation, the tank design needs to be self-cleaning so that the fish growth and welfare would not be negatively impacted. Hence, the practical implications of an incorrect tank design have profound effects on aquaculture operations. A common practice in the industry is to employ a particle trap near the outlet that receives approximately 1% or more of the total outflow. When a parcel of 500 particles with a specific gravity of 1.02 is released at the free-surface with an initial downward velocity of 1 cm/s, the distance between the despatch location to the domain exit in the case of elevated outlet is approximately double of that in the bottom outlet. To make a valid comparison for particle dynamics, only redesigns 2 and 3 with the same retention time of 55 min were examined where the outlet was on the tank's floor, but the inlets were near the sidewalls and corner walls, respectively. Particle breakup and surface roughness

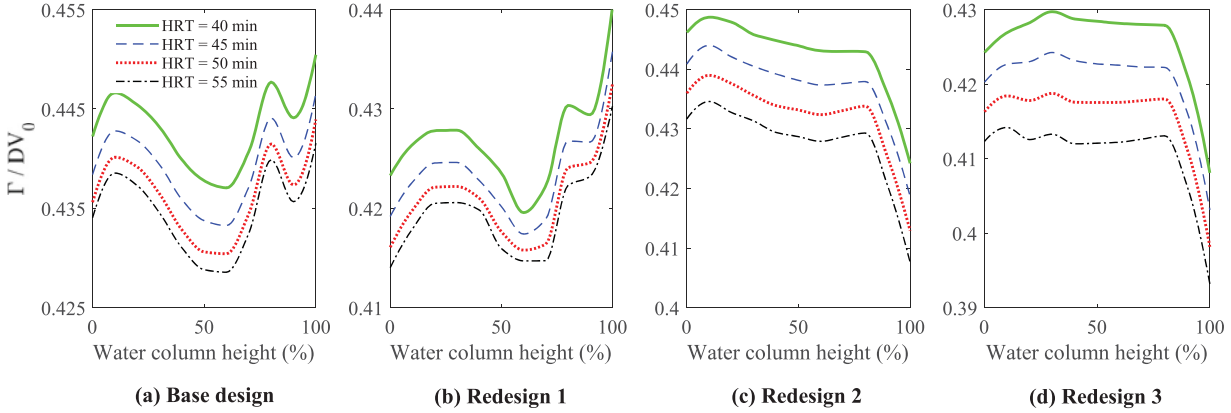

Fig. 13. Time-averaged vortex strength in the tank designs for different hydraulic retention times.

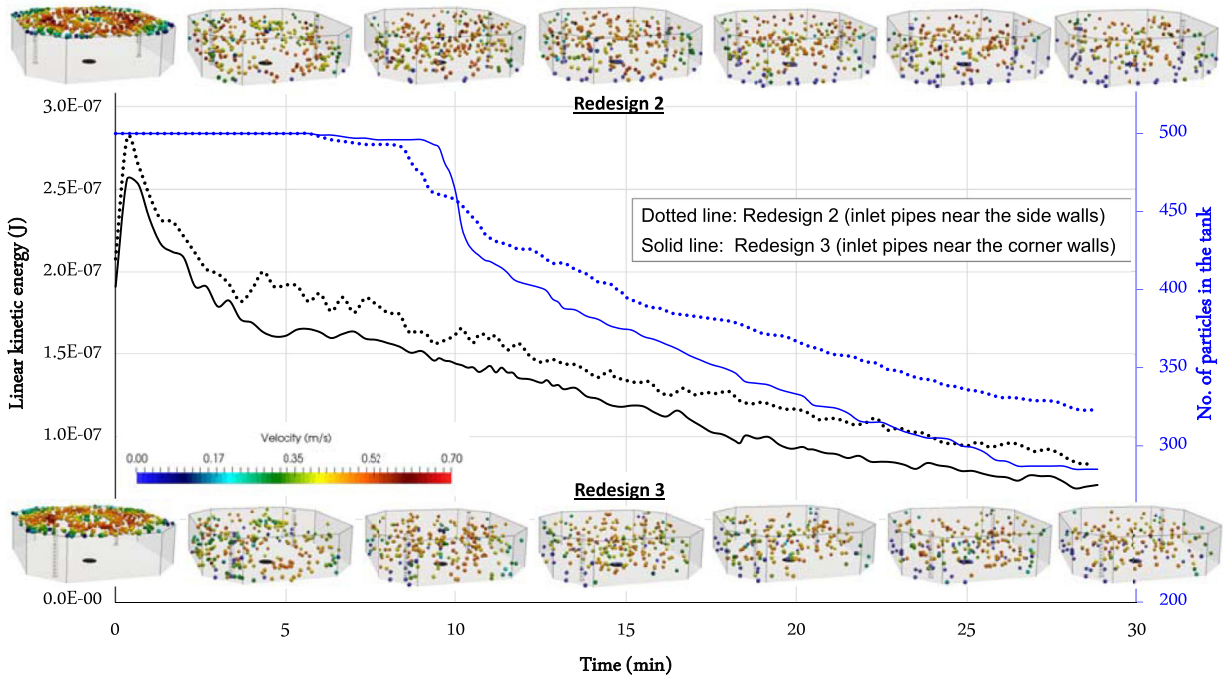

Fig. 14. Lagrangian parameters of the feed pellets in the tank with the inlets placed near the sidewalls (Redesign 2) and corner walls (Redesign 3). Both designs have the same outlet, which is on the tank's floor.

effects were ignored which did not affect the model accuracy as particles' motion is concerned. Fig. 14 presents the integrated information about the particle dispersion in the tank designs over a time of 30 min. With the early particle flushing within 7 min, Redesign 2 dominates its counterpart for about 10 min until 10% of particles are flushed. Around this time, with a sudden fall in the particle count, Redesign 3 has a sudden fall in the particle count and continues to exhibit a superior flushing activity to Redesign 2. A salmon culture tank with Redesign 3 is therefore safer for the fish and gives better welfare and performance, because there is less time for particles to disintegrate and produce water quality problems from the breakdown products of these particles. From the particle visuals, it can be seen that Redesign 2 has more static particles (in blue colour) on the floor than Redesign 3. As viewed from the time-history of linear kinetic energy, Redesign 2 creates a more fluctuating trend with a mean 18% more than Redesign 3. By the end of the considered duration, 18% more particles were left in Redesign 2, accounting for 14% higher kinetic energy than those in Redesign 3. Thus, moving the inlet pipes from the sidewall location to the corner walls would considerably improve the flushing action of biosolids in the existing tank.

4. Conclusions

Rapid solids flushing out of salmon culture tanks is a prerequisite for adequate fish welfare and fish performance. In this study, we show that inlet and outlet placements have a considerable impact on both solids' removal from the tank as well as the energy used to sustain the flow in the tank. Confined rotating flow in a large domain with a central outlet as in this case results in a complex combination of a large vortex column at the centre and a range of turbulent filaments around it. By moving the inlet pipes to the corner wall this provides advantages, such as the reduction in the drag force and local re-energization of the flow, when compared to the practice of inlet pipes placed near the sidewall. Regarding tank outlet design, the study showed that the

flow uniformity and circulation characteristics were better when using a flat bottom outlet than when using an elevated drain at the tank's centre. Also, it is concluded that, without changing the rearing volume and internal surface area, the mere shifting of inlet pipes close to the corner walls enhances the self-cleaning ability of the existing tank. By means of CFD-assisted design verification, the present study thus concluded that the *hydrodynamic positioning* of flow boundaries has a significant impact on the overall performance of the culture tank, which could potentially replace the existing practices of trial-and-error learning and experience-based approaches. In the long term, (re)designing culture tanks like this can provide a better environment for the fish, and thus result in improved fish welfare and health, and ultimately to more efficient salmon production.

Declaration of Competing Interest

On behalf of the coauthors, listed immediately below, I certify that they have NO affiliations with or involvement in any organization or entity with any financial interest (such as honoraria; educational grants; participation in speakers' bureaus; membership, employment, consultancies, stock ownership, or other equity interest; and expert testimony or patent-licensing arrangements), or non-financial interest (such as personal or professional relationships, affiliations, knowledge or beliefs) in the subject matter or materials discussed in this manuscript.

CRediT authorship contribution statement

JMR Gorle: Conceptualization, Data curation, Formal analysis, Investigation, Methodology, Project administration, Resources, Software, Validation, Visualization, Writing - original draft, Writing - review & editing. **BF Terjesen:** Conceptualization, Data curation, Formal analysis, Funding acquisition, Investigation, Methodology, Project administration, Resources, Supervision, Validation, Visualization, Writing - original draft, Writing - review & editing. **ST Summerfelt:** Conceptualization, Data curation, Formal analysis, Funding acquisition, Investigation, Methodology, Project administration, Resources, Supervision, Validation, Visualization, Writing - original draft, Writing - review & editing.

Acknowledgements

This research was part of the CtrlAQUA SFI, Centre for Closed-Containment Aquaculture, and funded by the Research Council of Norway (project #237856/O30) and the CtrlAQUA partners. Thanks to Marine Harvest for the cooperation and willingness to supply the design parameters of the RAS culture tank.

References

[1] Akbar MHM, Hayashi K, Lucas D, Tomiyama A. Effects of inlet condition on flow structure of bubbly flow in a rectangular column. Chem Eng Sci 2013;104:166–76. doi:10.1016/j.ces.2013.09.019.
[2] Ardiansyah A, Fotedar R. Water quality, growth and stress responses of juvenile barramundi (Lates calcarifer Bloch), reared at four different densities in integrated recirculating aquaculture systems. Aquaculture 2016;458:113–20. doi:10.1016/j.aquaculture.2016.03.001.
[3] Asif MA, Gupta AD, Rana MDJ, Ahmed DH. Investigation of drag reduction through a flapping mechanism on circular cylinder. AIP Conf Proc 2016;1754:040014. doi:10.1063/1.4958374.
[4] Balachandar S, Eaton JK. Turbulent dispersed multiphase flow. Annu Rev Fluid Mech 2010;42:111–33. doi:10.1146/annurev.fluid.010908.165243.
[5] Bechtold M, Vanderborght J, Ippisch O, Vereecken H. Efficient random walk particle tracking algorithm for advective-dispersive transport in media with discontinuous dispersion coefficients and water contents. Water Resour Res 2011;47(10):W10526. doi:10.1029/2010WR010267.
[6] Bernardini M, Pirozzoli S, Orlandi P. The effect of large-scale turbulent structures on particle dispersion in wall-bounded flows. Int J Mult Flow 2013;51:55–64. doi:10.1016/j.ijmultiphaseflow.2012.11.007.
[7] Butt U, Jehring L, Egbers C. Mechanism of drag reduction for circular cylinders with patterned surface. Int J Heat Fluid Flow 2014;45:128–34. doi:10.1016/j.ijheatfluidflow.2013.10.008.
[8] Chen J, Wang J, Ma J. Effects of gas flow-rate and inlet concentration on nitric oxide removal in an autotrophic biofilter. J Chem Technol Biotechnol 2006;81(5):812–16. doi:10.1002/jctb.1463.
[9] Cheng N-S. Calculation of drag coefficient for arrays of emergent circular cylinders with pseudofluid model. J Hydraul. Eng. 2013;139(6):602–11. doi:10.1061/(ASCE)HY.1943-7900.0000722.
[10] Crowe CT. Review - numerical models for dilute gas-particle flows. J Fluids Eng 1982;104(3):297–303. doi:10.1115/1.3241835.
[11] Da Silva CB, Metais O. On the influence of coherent structures upon interscale interactions in turbulent plane jets. J Fluid Mech 2002;473:103–45. doi:10.1017/S0022112002002458.
[12] Dalsgaard J, Lund L, Thorarinsdottir R, Drengstig A, Arvonen K, Pedersen PB. Farming different species in RAS in Nordic countries: current status and future perspectives. Aquacult Eng 2013;53:2–13. doi:10.1016/j.aquaeng.2012.11.008.
[13] Davidson J, Good C, welsh C, Summerfelt ST. The effects of ozone and water exchange rates on water quality and rainbow trout Oncorhynchus mykiss performance in replicated water reuse systems. Aquacult Eng 2011;44:80–96. doi:10.1016/j.aquaeng.2011.04.001.
[14] Davidson J, Summerfelt ST. Solids flushing, mixing, and water velocity profiles within large (10 and 150 m3) circular 'Cornell-type' dual-drain tanks. Aquacult Eng 2004;32(1):245–71. doi:10.1016/j.aquaeng.2004.03.009.
[15] Davidson J, Summerfelt ST. Solids removal from a coldwater recirculating system - comparison of a swirl separator and a radial-flow settler. Aquacult Eng 2005;33(1):47–61. doi:10.1016/j.aquaeng.2004.11.002.
[16] Davidson J, Summerfelt R, Barrows F, Gottsacker B, Good C, Fischer G, Summerfelt ST. Walleye Sander vitreus performance, water quality, and waste production in replicated recirculation aquaculture systems when feeding a low phosphorus diet without fishmeal versus a traditional fishmeal-based diet. Aquacult Eng 2016;75:1–13. doi:10.1016/j.aquaeng.2016.09.005.
[17] Dombroski DE, Crimaldi J. The accuracy of acoustic Doppler velocimetry (ADV) measurements in turbulent boundary layer flows over a smooth bed. Limnol Oceanogr Methods 2007;5(1):23–33. doi:10.4319/lom.2007.5.23.
[18] Elghobashi S. On predicting particle laden turbulent flows. Appl Sci Res 1994;52:309–29. doi:10.1007/BF00936835.
[19] Espmark AM, Kolarevic J, Asgard T, Terjesen BF. Tank size and fish management history matters in experimental design. Aquac Res 2016;48(6):2876–94. doi:10.1111/are.13121.
[20] Freund JB, Mungal MG. Drag and wake modification of axisymmetric bluff bodies using Coanda blowing. J Aircr 1994;31(3):572–8. doi:10.2514/3.46532.
[21] Golkarfard V, Talebizadeh P. Numerical comparison of airborne particles deposition and dispersion in radiator and floor heating systems. Adv Powder Technol 2014;25(1):389–97. doi:10.1016/j.apt.2013.06.008.
[22] Good C, Davidson J, Earley RL, Styga J, Summerfelt ST. The effects of ozonation on select waterborne steroid hormones in recirculation aquaculture systems containing sexually mature Atlantic salmon Salmo salar. Aquacult Eng 2017;79:9–16. doi:10.1016/j.aquaeng.2017.08.004.
[23] Good C, Davidson J, Terjesen BF, Takle H, Kolarevic J, Baeverfjord G, Summerfelt ST. The effects of long-term 20 mg/L carbon dioxide exposure on the health and performance of Atlantic salmon Salmo salar post-smolts in water recirculation aquaculture systems. Aquacult Eng 2018;81:1–9. doi:10.1016/j.aquaeng.2018.01.003.
[24] Gorle JMR, Chatellier L, Pons F, Ba M. Flow and performance analysis of H-Darrieus hydroturbine in a confined flow: a computational and experimental study. J Fluids Struct 2016;66:382–402. doi:10.1016/j.jfluidstructs.2016.08.003.
[25] Gorle JMR, Terjesen BF, Holan AB, Berge A, Summerfelt ST. Qualifying the design of a floating closed-containment fish farm using computational fluid dynamics. Biosyst Eng 2018;175:63–81. doi:10.1016/j.biosystemseng.2018.08.012.
[26] Gorle JMR, Terjesen BF, Mota VC, Summerfelt ST. Water velocity in commercial RAS culture tanks for Atlantic salmon smolt production. Aquacult Eng 2018;81:89–100. doi:10.1016/j.aquaeng.2018.03.001.
[27] Gorle JMR, Terjesen BF, Summerfelt ST. Hydrodynamics of octagonal culture tanks with Cornell-type dual-drain system. Comput Electr Agric 2018;151:354–64. doi:10.1016/j.compag.2018.06.012.
[28] Gorle JMR, Terjesen BF, Summerfelt ST. Hydrodynamics of Atlantic salmon culture tank: effect of inlet nozzle angle on the velocity field. Comput Electr Agric 2019;158:79–91. doi:10.1016/j.compag.2019.01.046.
[29] Hagspiel V, Hannevik J, Lavrutich M, Naustdal M, Struksnæs H. Real options under technological uncertainty: a case study of investment in a post-smolt facility in Norway. Mar Policy 2018;88:158–66. doi:10.1016/j.marpol.2017.11.020.
[30] Hendrick P, Degrez G. Numerical and experimental investigation of slot-blown air over a cylinder. Progress in Flight Phys 2015;7:229–44. doi:10.1051/eucass/201507229.
[31] James SE, Suryan A, Sebastian JJ, Mohan A, Kim HD. Comparative study of boundary layer control around an ordinary airfoil and a high lift airfoil with secondary blowing. Comput Fluids 2018;164:50–63. doi:10.1016/j.compfluid.2017.03.012.
[32] Letelier-Gordo CO, Aalto SL, Suurnäkki S, Pedersen PB. Increased sulfate availability in saline water promotes hydrogen sulfide production in fish organic waste. Aquacult Eng 2020;89:102062. doi:10.1016/j.aquaeng.2020.102062.
[33] Marchioli C, Soldati A. Mechanisms for particle transfer and segregation in a turbulent boundary layer. J Fluid Mech 2002;468:283–315. doi:10.1017/S0022112002001738.
[34] Masalo I, Oca J. Hydrodynamics in a multivortex aquaculture tank: Effect of baffles and water inlet characteristics. Aquacult Eng 2014;58:69–76. doi:10.1016/j.aquaeng.2013.11.001.
[35] Maurina GZ, Da Rosa LM, Beal LL, Torres AP, Sousa M. Numerical study of different inlet configurations on the fluid dynamics of an anaerobic sequencing batch reactor. Chem Eng Trans 2014;38:127–32. doi:10.3303/CET1438022.

[36] McMurtry MR, Nelson PV, Sanders DC, Hodges L. Effects of biofilter/culture tank volume ratios on productivity of a recirculating fish/vegetable co-culture system. J Appl Aquacult 1997;7(4):33–51. doi:10.1300/J028v07n04_03.
[37] Morize C, Moisy F. Energy decay of rotating turbulence with confinement effects. Phys Fluids 2006;18(6):065107. doi:10.1063/1.2212990.
[38] Nordin N, Seri SM, Taib I, Mohammed AN, Abdullah MK, Sapit A. Secondary flow vortices and flow separation of 2-D turning diffuser via particle image velocimetry. IOP Conf. Series: Mater Sci Eng 2017;22:012149. doi:10.1088/1757-899X/226/1/012149.
[39] Oca J, Masalo I. Design criteria for rotating flow cells in rectangular aquaculture tanks. Aquacult Eng 2007;36:36–44. doi:10.1016/j.aquaeng.2006.06.001.
[40] Oca J, Masalo I. Flow pattern in aquaculture circular tanks: Influence of flow rate, water depth, and water inlet & outlet features. Aquacult Eng 2013;52:65–72. doi:10.1016/j.aquaeng.2012.09.002.
[41] Park T, Sung Y, Kim T, Lee I, Choi G, Kim D. Effect of static mixer geometry on flow mixing and pressure drop in marine SCR applications. Int J Naval Arch Ocean Eng 2014;6(1):27–38. doi:10.2478/IJNAOE-2013-0161.
[42] Plew DR, Klebert P, Rosten TW, Aspaas S, Birkevold J. Changes to flow and turbulence caused by different concentrations of fish in a circular tank. J Hydraul Res 2015;53(3):364–83. doi:10.1080/00221686.2015.1029016.
[43] Pope SB. Turbulent flows. Cambridge: Cambridge University Press; 2000.
[44] Prabhu PAJ, Kaushik S, Geurden I, Stouten T, Dicharry SF, Veron V, Mariojouls C, Verreth JAJ, Eding EH, Schrama JW. Water exchange rate in RAS and dietary inclusion of micro-minerals influence growth, body composition and mineral metabolism in common carp. Aquaculture 2017;471:8–18. doi:10.1016/j.aquaculture.2016.12.031.
[45] Qiu T, Qi J, Zheng J, Liu Y. Design and performance of a recirculating aquaculture system for oyster larval culture. Aquac Res 2017;48(12):5699–706. doi:10.1111/are.13392.
[46] Rud I, Kolarevic J, Holan AB, Berget I, Calabrese S, Terjesen BF. Deep-sequencing of the bacterial microbiota in commercial-scale recirculating and semi-closed aquaculture systems for Atlantic salmon post-smolt production. Aquacult Eng 2017;78:50–62. doi:10.1016/j.aquaeng.2016.10.003.
[47] Schlichting H. Boundary layer theory. 1st ed. New York: McGraw-Hill; 1955.
[48] Schlatter P, Orlu R. Quantifying the interaction between large and small scales in wall-bounded turbulent flows: a note of caution. Phys Fluids 2010;22:051704. doi:10.1063/1.3432488.
[49] Schrader KK, Davidson JW, Rimando AM, Summerfelt ST. Evaluation of ozonation on levels of the off-flavor compounds geosmin and 2-methylisoborneol in water and rainbow trout Oncorhynchus mykiss from recirculating aquaculture systems. Aquacult Eng 2010;43:46–50. doi:10.1016/j.aquaeng.2010.05.003.
[50] Summerfelt ST, Davidson J, Wilson G, Waldrop T. Advances in fish harvest technologies for circular tanks. Aquacult Eng 2009;40(2):62–71. doi:10.1016/j.aquaeng.2008.12.001.
[51] Summerfelt ST, Mathisen F, Holan AB, Terjesen BF. Survey of large circular and octagonal tanks operated at Norwegian commercial smolt and post-smolt sites. Aquacult Eng 2016;74:105–10. doi:10.1016/j.aquaeng.2016.07.004.
[52] Summerfelt ST, Wilton G, Roberts D, Savage T-M, Fonkalsrud K. Developments in recirculating systems for Arctic char culture in North America. Aquacult Eng 2004;30(1-2):31–71. doi:10.1016/j.aquaeng.2003.09.001.
[53] Summerfelt ST, Vinci BJ. Better management practices for recirculating systems. In: Tucker CS, Hargreaves JA, editors. Environmental best management practices for aquaculture. Ames: Blackwell Publishing; 2008. p. 389–426.
[54] Talebizadeh P, Rahimzadeh H, Ahmadi G, Brown R, Inthavong K. Time history of diesel particle deposition in cylindrical dielectric barrier discharge reactors. J Nanoparticle Res 2016;18:378. doi:10.1007/s11051-016-3667-8.
[55] Terjesen BF, Summerfelt ST, Nerland S, Ulgenes Y, Fjæra SO, Megård Reiten BK, Selset R, Kolarevic J, Brunsvik P, Bæverfjord G, Takle H, Kittelsen A, Åsgård T. Design, dimensioning, and performance of a research facility for studies on the requirements of fish in RAS environments. Aquacult Eng 2013;54:49–63. doi:10.1016/j.aquaeng.2012.11.002.
[56] Velasco D, Mejia OL, Lain S. Numerical simulations of active flow control with synthetic jets in a Darrieus turbine. Renew Energy 2017;113:129–40. doi:10.1016/j.renene.2017.05.075.
[57] Wieselsberger C. New data on the laws of fluid resistance. National Advisory Committee for Aeronautics; 1922. Technical Note No. 84.
[58] Yao J, Fairweather M. Particle deposition in turbulent duct flows. Chem Eng Sci 2012;84:781–800. doi:10.1016/j.ces.2012.09.020.
[59] Ye Z, Wang S, Gao W, Li H, Pei L, Shen M, Zhu S. Synergistic effects of microelectrolysis-photocatalysis on water treatment and fish performance in saline recirculating aquaculture system. Sci Rep 2017;7:45066. doi:10.1038/srep45066.
[60] Ytrestøyl T, Takle H, Kolarevic J, Calabrese S, Timmerhaus G, Rosseland BO, Teien HC, Nilsen TO, Handeland SO, Stefansson SO, Ebbesson LOE, Terjesen BF. Performance and welfare of Atlantic salmon, Salmo salar L. post-smolts in recirculating aquaculture systems: Importance of salinity and water velocity. J World Aquac Soc 2020:1–20. doi:10.1111/jwas.12682.